

Cite this: DOI: 00.0000/xxxxxxxxxx

Plateau-Rayleigh instability of a soft layer coated on a rigid cylinder

Bharti, Andreas Carlson and Tak Shing Chan*

Received Date
Accepted Date

DOI: 00.0000/xxxxxxxxxx

We study the Plateau-Rayleigh instability of a viscoelastic soft solid layer coated on a rigid cylinder i.e., a soft fibre with a rigid core. The onset of instability is examined using a linear stability analysis. We find that increasing the rigid cylinder radius reduce the growth rate of the fastest growing mode. For each rigid cylinder radius, a critical elastocapillary number is found below which all wavelengths of disturbances are stable. The critical value for a soft fibre with a thick rigid cylindrical core can be several orders of magnitudes larger than that for a totally soft fibre (no rigid core), which highlights the strong stabilizing effect of the rigid core on the system. Increasing the relaxation timescale of the viscoelastic material also slows down the growth of disturbance, but has no effect on the critical elastocapillary number. Interestingly, the wavelength of the fastest growing mode is independent of the rigid cylinder radius for the purely elastic case.

1 Introduction

Significant stress is usually required for a solid to deform, and as such the effects due to surface tension have often been ignored. Soft solids such as elastomers and gels¹, on the other hand, have elastic moduli ranging between kPa to MPa, which means they can deform much easier. In recent years, there has been significant attention to how capillary effects can lead to soft solid deformations, and fascinating elastocapillary phenomena have been discovered^{2–6}. The Plateau-Rayleigh instability (PRI)^{7,8}, namely the instability driven by surface tension and often illustrated by the breaking up of liquid jets into droplets⁹, has currently been examined for fibres made of soft solids^{10–19}.

Studies of the PRI of soft fibres have focused on soft materials that demonstrate elastic or viscoelastic responses^{10–19}. An experimental study using soft agar gel fibres by Mora et al.¹² has shown that the instability occurs when the elastocapillary length $\gamma/\mu \geq 6R$, where R is the radius of the soft fibre, γ is the solid surface tension and μ is the shear modulus. Other studies of the PRI on a soft fibre include, for example, the formation of beads-on-string structures^{10,14,16,20}. Another interesting factor that might significantly modify the instability is having an inner rigid core, i.e. a fibre consists of a soft-layer-coated on a rigid cylinder. Such kind of setup, but with a coated liquid film instead of a soft solid layer, has been studied extensively^{21–30} since the early works in the 1960s by Goren^{31,32}. To name a few, some studies address the effects of liquid slip on solid surface^{26,30} and the dynamics

of the droplets formed on the fibre²³. However, there has been a lack of investigations on situations in which the coated layer is a soft solid. How viscoelastic properties and the rigid core influence the PRI of a soft-layer-coated fibre remain unclear, which is addressed in this article.

Soft solids have nowadays been used in many applications, for example in 3D bioprinting³³, mimicking muscle tissues in biomedicine³⁴ and water harvesting³⁵. In living organisms, soft fibrous-shaped structures are often found in cellular tubes and compartments of cells. Instability of these biological ingredients resembling to the PRI has been observed^{36–40}. One example is a recent study on the undulation and droplet formation of a layer of condensed protein TPX2 on a microtubule⁴⁰. Hence, investigating the PRI of fibrous soft solids is becoming more important for both understanding the fundamental physical problems and the development of new technologies. In this study, we examine the onset of PRI of a soft layer coated on a rigid cylinder through a linear stability analysis.

2 Formulation

We consider a rigid cylinder of radius r_0 coated with a layer of incompressible viscoelastic material of uniform thickness H at an undeformed state. The whole fibre consisting of the rigid cylinder and the coated soft layer has a total radius $R = r_0 + H$ as shown in Fig.1. By neglecting all body forces (e.g. gravity) and only considering viscoelastic stresses, the equation of motion of a soft material element of density ρ is given by

$$\frac{\partial \sigma_{ij}(\mathbf{x}, t)}{\partial x_j} = \rho \frac{\partial^2 u_i(\mathbf{x}, t)}{\partial t^2} \quad (1)$$

^a Mechanics Division, Department of Mathematics, University of Oslo, 0316 Oslo, Norway. Email: taksc@uio.no

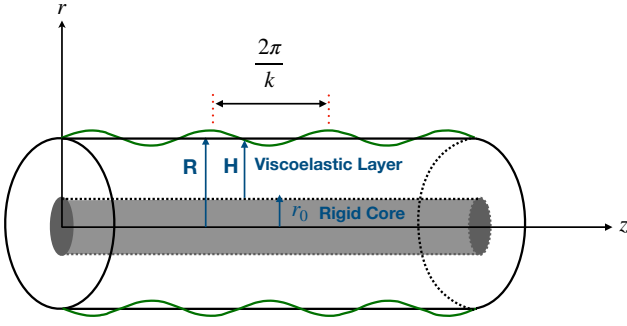


Fig. 1 Schematic representation of an infinitely long, rigid cylinder of radius r_0 coated with a layer of incompressible viscoelastic material of uniform thickness H at an undeformed state. A random disturbance of the interface of the viscoelastic layer is decomposed into sinusoidal deformations of wavenumber k . In cylindrical coordinates systems, r and z are respectively the radial coordinate and the longitudinal coordinate.

where $\sigma_{ij}(\mathbf{x}, t)$ and $u_i(\mathbf{x}, t)$ are respectively the stress tensor and the displacement vector in index notation at a position vector \mathbf{x} and time t . Assuming a linear viscoelastic response of the incompressible soft material, the relation between σ_{ij} and the strain tensor ε_{ij} is

$$\sigma_{ij}(\mathbf{x}, t) = 2 \int_{-\infty}^t \mu(t-t') \frac{\partial \varepsilon_{ij}(\mathbf{x}, t')}{\partial t'} dt' - p(\mathbf{x}, t) \delta_{ij}, \quad (2)$$

where $\mu(t)$ is the shear relaxation function, p is the pressure, δ_{ij} is the Kronecker delta, and the strain tensor ε_{ij} is related to the displacement as

$$\varepsilon_{ij} = \frac{1}{2} \left(\frac{\partial u_i}{\partial x_j} + \frac{\partial u_j}{\partial x_i} \right). \quad (3)$$

There are different models that have been used to describe viscoelastic materials. The simplest models are the Kelvin-Voigt model or the Maxwell model, which consists of a spring and a viscous damper connected in parallel or in series respectively. In this study, we consider the soft material to behave as a gel described by the Chasset-Thirion model assuming a power law response given by

$$\mu(t) = \mu_0 \left[1 + \Gamma(1-n)^{-1} \left(\frac{\tau}{t} \right)^n \right], \quad (4)$$

where μ_0 is the static shear modulus, τ is the relaxation timescale of the viscoelastic response, Γ is the gamma function and n is a parameter typically smaller than or equal to unity.

To compute the growth rate of disturbance on the viscoelastic layer, we follow the approach delineated by previous studies^{15,30}. We decompose the time-dependent variables into normal modes e^{st} , where s is the growth rate. The amplitude of the normal mode of a function $f(t)$ is obtained by the Laplace transform defined as

$$\tilde{f}(s) = \int_0^{\infty} f(t) e^{-st} dt. \quad (5)$$

We apply the Laplace transform to the constitutive relation (2)

and obtain

$$\tilde{\sigma}_{ij}(\mathbf{x}, s) = \hat{\mu}(s) \left[\frac{\partial \tilde{u}_i(\mathbf{x}, s)}{\partial x_j} + \frac{\partial \tilde{u}_j(\mathbf{x}, s)}{\partial x_i} \right] - \tilde{p}(\mathbf{x}, s) \delta_{ij} \quad (6)$$

where $\tilde{\sigma}_{ij}$, \tilde{u}_i and \tilde{p} are respectively the Laplace transform of σ_{ij} , u_i and p , and $\hat{\mu}(s)$ is the shear modulus in Laplace space defined as

$$\hat{\mu}(s) \equiv s \int_0^{\infty} \mu(t) e^{-st} dt = \mu_0 [1 + (s\tau)^n]. \quad (7)$$

Thus the governing equation (1) in Laplace space can be written as

$$\hat{\mu}(s) \frac{\partial^2 \tilde{u}_i}{\partial x_j \partial x_j} - \frac{\partial \tilde{p}}{\partial x_i} = \rho s^2 \tilde{u}_i. \quad (8)$$

Next, we scale the lengths with the radius of the whole fibre R , the time with the capillary timescale $\sqrt{\rho R^3 / \gamma}$ and the stresses by μ_0 . We define the following dimensionless variables as

$$\bar{r} = \frac{r}{R}, \quad \bar{z} = \frac{z}{R}, \quad \bar{s} = \sqrt{\frac{\rho R^3}{\gamma}} s, \quad (9)$$

$$\bar{u}_i(\bar{r}, \bar{z}, \bar{s}) = \frac{\tilde{u}_i}{R}, \quad \bar{p}(\bar{r}, \bar{z}, \bar{s}) = \frac{\tilde{p}}{\mu_0}, \quad \bar{\sigma}_{ij}(\bar{r}, \bar{z}, \bar{s}) = \frac{\tilde{\sigma}_{ij}}{\mu_0}. \quad (10)$$

The dimensionless form of the governing equation (eq. 8) in Laplace space is

$$\left[1 + (\bar{\tau} \bar{s})^n \right] \frac{\partial^2 \bar{u}_i}{\partial x_j \partial x_j} - \frac{\partial \bar{p}}{\partial x_i} = \Sigma \bar{s}^2 \bar{u}_i \quad (11)$$

where $\bar{\tau} = \tau / \sqrt{\rho R^3 / \gamma}$ and the elastocapillary number $\Sigma = \gamma / (\mu_0 R)$.

We consider only the longitudinal disturbance and neglect the azimuthal disturbance as azimuthal normal modes always increase the surface energy⁹. The deformation of the soft layer is axisymmetric. We hence use the cylindrical coordinate system (r, ϕ, z) and the corresponding unit vectors are denoted as $(\hat{r}, \hat{\phi}, \hat{z})$. The displacement vector is denoted as $\mathbf{u}(r, z, t) = u_r(r, z, t) \hat{r} + u_z(r, z, t) \hat{z}$. Note that $u_\phi = 0$ due to axisymmetry.

The governing equation (11) can be solved by applying the Helmholtz decomposition of the displacement as described in the references^{15,30}. The general solutions are given as

$$\bar{p}(\bar{s}) = -\bar{s}^2 \Sigma \left[A_1 I_0(\bar{k} \bar{r}) + A_3 K_0(\bar{k} \bar{r}) \right] e^{i \bar{k} \bar{z}}, \quad (12)$$

$$\bar{u}_r = \left[A_1 \bar{k} I_1(\bar{k} \bar{r}) - A_2 (i \bar{k}) I_1(\alpha \bar{r}) - A_3 \bar{k} K_1(\bar{k} \bar{r}) - A_4 (i \bar{k}) K_1(\alpha \bar{r}) \right] e^{i \bar{k} \bar{z}}, \quad (13)$$

and

$$\bar{u}_z = \left[A_1 (i \bar{k}) I_0(\bar{k} \bar{r}) + A_2 \alpha I_0(\alpha \bar{r}) + A_3 (i \bar{k}) K_0(\bar{k} \bar{r}) - A_4 \alpha K_0(\alpha \bar{r}) \right] e^{i \bar{k} \bar{z}} \quad (14)$$

where $\bar{k} \equiv kR$ is the dimensionless wavenumber, I and K are respectively the modified Bessel functions of the first and second kind, $\alpha = \sqrt{\bar{s}^2 \beta + \bar{k}^2}$, $\beta = \Sigma / (1 + (\bar{\tau} \bar{s})^n)$ and $A_m (m = 1, 2, 3, 4)$ are the undermined coefficients.

Next we impose the boundary conditions. At $\bar{r} = \bar{r}_0 \equiv r_0/R$, there is no penetration of material, thus

$$\bar{u}_r|_{\bar{r}=\bar{r}_0} = 0. \quad (15)$$

For the z-direction, we impose a no-displacement condition

$$\bar{u}_z|_{\bar{r}=\bar{r}_0} = 0. \quad (16)$$

At $\bar{r} = 1$, we assume the slope of the deformed interface to be small. Balancing the Laplace pressure due to solid surface tension and the viscoelastic stresses gives

$$\bar{\sigma}_{rr}|_{\bar{r}=1} = \Sigma \left(\frac{\partial^2 \bar{u}_r}{\partial \bar{z}^2} + \bar{u}_r \right) |_{\bar{r}=1}, \quad (17)$$

in r-direction, and gives the vanishing shear stress

$$\bar{\sigma}_{rz}|_{\bar{r}=1} = 0 \quad (18)$$

in z-direction.

3 Dispersion relation

Using the expressions of the general solutions (eq. 12-14) for the boundary conditions (eq. 15-18) yields the following set of linear equations for the unknowns A_m .

$$A_1 \bar{k} I_1(\bar{r}_0 \bar{k}) - A_2 i \bar{k} I_1(\bar{r}_0 \alpha) - A_3 \bar{k} K_1(\bar{r}_0 \bar{k}) - A_4 i \bar{k} K_1(\bar{r}_0 \alpha) = 0, \quad (19)$$

$$A_1 (i \bar{k}) I_0(\bar{r}_0 \bar{k}) + A_2 \alpha I_0(\bar{r}_0 \alpha) + A_3 (i \bar{k}) K_0(\bar{r}_0 \bar{k}) - A_4 \alpha K_0(\bar{r}_0 \alpha) = 0, \quad (20)$$

$$\begin{aligned} & A_1 \left\{ \frac{\alpha^2 + \bar{k}^2}{2} I_0(\bar{k}) - \bar{k} I_1(\bar{k}) - \frac{\beta}{2} (1 - \bar{k}^2) \bar{k} I_1(\bar{k}) \right\} \\ & + A_2 \left\{ -i \bar{k} [\alpha I_0(\alpha) - I_1(\alpha)] + \frac{\beta}{2} i \bar{k} (1 - \bar{k}^2) I_1(\alpha) \right\} \\ & + A_3 \left\{ \frac{\alpha^2 + \bar{k}^2}{2} K_0(\bar{k}) + \bar{k} K_1(\bar{k}) + \frac{\beta}{2} (1 - \bar{k}^2) \bar{k} K_1(\bar{k}) \right\} \\ & + A_4 \left\{ i \bar{k} [\alpha K_0(\alpha) + K_1(\alpha)] + \frac{\beta}{2} i \bar{k} (1 - \bar{k}^2) K_1(\alpha) \right\} = 0, \end{aligned} \quad (21)$$

and

$$\begin{aligned} & A_1 2i \bar{k}^2 I_1(\bar{k}) + A_2 (\bar{k}^2 + \alpha^2) I_1(\alpha) - A_3 2i \bar{k}^2 K_1(\bar{k}) \\ & + A_4 (\bar{k}^2 + \alpha^2) K_1(\alpha) = 0. \end{aligned} \quad (22)$$

The solvability condition for non-trivial solutions of the linear equations with unknowns A_m is that the determinant is vanishing, which gives the following dispersion relation

$$\begin{vmatrix} \bar{k} I_1(\bar{r}_0 \bar{k}) & -i \bar{k} I_1(\bar{r}_0 \alpha) & -\bar{k} K_1(\bar{r}_0 \bar{k}) & -i \bar{k} K_1(\bar{r}_0 \alpha) \\ (i \bar{k}) I_0(\bar{r}_0 \bar{k}) & \alpha I_0(\bar{r}_0 \alpha) & (i \bar{k}) K_0(\bar{r}_0 \bar{k}) & -\alpha K_0(\bar{r}_0 \alpha) \\ C_1 & C_2 & C_3 & C_4 \\ 2i \bar{k}^2 I_1(\bar{k}) & (\bar{k}^2 + \alpha^2) I_1(\alpha) & -2i \bar{k}^2 K_1(\bar{k}) & (\bar{k}^2 + \alpha^2) K_1(\alpha) \end{vmatrix} = 0, \quad (23)$$

where

$$\begin{aligned} C_1 &= \frac{\alpha^2 + \bar{k}^2}{2} I_0(\bar{k}) - \bar{k} I_1(\bar{k}) - \frac{\beta}{2} (1 - \bar{k}^2) \bar{k} I_1(\bar{k}), \\ C_2 &= -i \bar{k} [\alpha I_0(\alpha) - I_1(\alpha)] + \frac{\beta}{2} i \bar{k} (1 - \bar{k}^2) I_1(\alpha), \\ C_3 &= \frac{\alpha^2 + \bar{k}^2}{2} K_0(\bar{k}) + \bar{k} K_1(\bar{k}) + \frac{\beta}{2} (1 - \bar{k}^2) \bar{k} K_1(\bar{k}), \end{aligned}$$

$$C_4 = i \bar{k} (\alpha K_0(\alpha) + K_1(\alpha)) + \frac{\beta}{2} i \bar{k} (1 - \bar{k}^2) K_1(\alpha).$$

The dimensionless control parameters are: \bar{r}_0 , Σ , $\bar{\tau}$ and n .

4 Results

The validation of the dispersion relation (eq. 23) is presented in the Appendix in which we compare our results in the Newtonian fluid limit with some previous studies. In this section, we first consider the purely elastic solid limit and then we focus on the effects of viscoelasticity.

4.1 The purely elastic solid limit

When the viscoelastic relaxation timescale τ is small compared to the time scale $\sqrt{\rho R^3/\gamma}$, i.e. taking the limit $\bar{\tau} \rightarrow 0$, our viscoelastic model reduces to the purely elastic model. In this limit, $\alpha = \sqrt{\bar{s}^2 \Sigma + \bar{k}^2}$ and $\beta = \Sigma$ in the dispersion relation (eq. 23). We examine how the instability depends on the dimensionless parameters Σ and \bar{r}_0 .

4.1.1 Dependence on the rigid core radius and the elastocapillary number

We show the dispersion relation (eq. 23) by plotting the dimensionless growth rate \bar{s} as a function of the dimensionless wavenumber \bar{k} for different values of Σ and a fixed $\bar{r}_0 = 0.1$ in Fig. 2 (a). We see that for each curve, the unstable modes (i.e. $\bar{s} > 0$) lie within a certain range of dimensionless wavenumber, i.e. $\bar{k}_1 < \bar{k} < \bar{k}_2$, where \bar{k}_1 and \bar{k}_2 are defined as $\bar{s}(\bar{k}_1) = 0$ and $\bar{s}(\bar{k}_2) = 0$. Within each range of unstable modes, there is a dimensionless wavenumber $\bar{k} = \bar{k}_m$ that corresponds to the fastest growing mode with a maximum dimensionless growth rate $\bar{s}_m \equiv \bar{s}(\bar{k} = \bar{k}_m)$. To study how the characteristic quantities depend on the control parameters, we plot \bar{s}_m , \bar{k}_m , and \bar{k}_1 (and \bar{k}_2) as a function of Σ respectively in Fig. 2 (b), (c) and (d) for three different dimensionless rigid core radius, i.e. $\bar{r}_0 = 10^{-9}$, $\bar{r}_0 = 0.1$ and 0.9 . We also add the result from Tamim *et al.*¹⁵ for the situation of a soft fibre without a rigid cylindrical core (i.e. $\bar{r}_0 = 0$). We see in Fig. 2 (b) that for all four different \bar{r}_0 , the dimensionless growth rate of the fastest growing mode \bar{s}_m decreases with decreasing Σ . When Σ is reduced to a critical value Σ_c , \bar{s}_m drops to zero. There is no positive solution of \bar{s} for $\Sigma < \Sigma_c$. It means the coated elastic layer is stable under disturbance of any wavelength when $\Sigma < \Sigma_c$. We would also point out that, first, the critical value Σ_c for $\bar{r}_0 = 0.9$ is orders of magnitude larger than that for $\bar{r}_0 = 0.1$. Second, even for the rigid cylindrical core radius as small as $\bar{r}_0 = 10^{-9}$, there is a slight difference from the result for $\bar{r}_0 = 0$ when Σ is close to Σ_c . A stability phase diagram of Σ_c vs \bar{r}_0 will be examined in section 4.1.2. Interestingly, as shown in Fig. 2 (c), we find that the dimensionless wavenumber of the fastest growing mode \bar{k}_m is independent of the dimensionless radius of the rigid core \bar{r}_0 , and decreases with reducing Σ . When $\Sigma \rightarrow \infty$, we find $\bar{k}_m = 0.7$, which agrees with the dimensionless wavenumber of the fastest growing mode for the classical PRI of inviscid fluid jet^{8,9}. Another remarkable point is that \bar{k}_m starts to drop significantly with reducing Σ only when $\Sigma \lesssim 10^2$. For cases with $\Sigma_c > 10^2$, e.g. for $\bar{r}_0 = 0.9$, the dimensionless wavenumber of the fastest growing mode is always close to the asymptotic value, i.e. $\bar{k}_m \approx 0.68$. Regarding the range

of unstable modes, as we can see in Fig. 2 (a) and Fig. 2 (d), it shrinks when Σ is reduced. Namely, \bar{k}_1 increases (or remains zero for $\bar{r}_0 = 0$) and \bar{k}_2 decreases.

4.1.2 Stability phase diagram

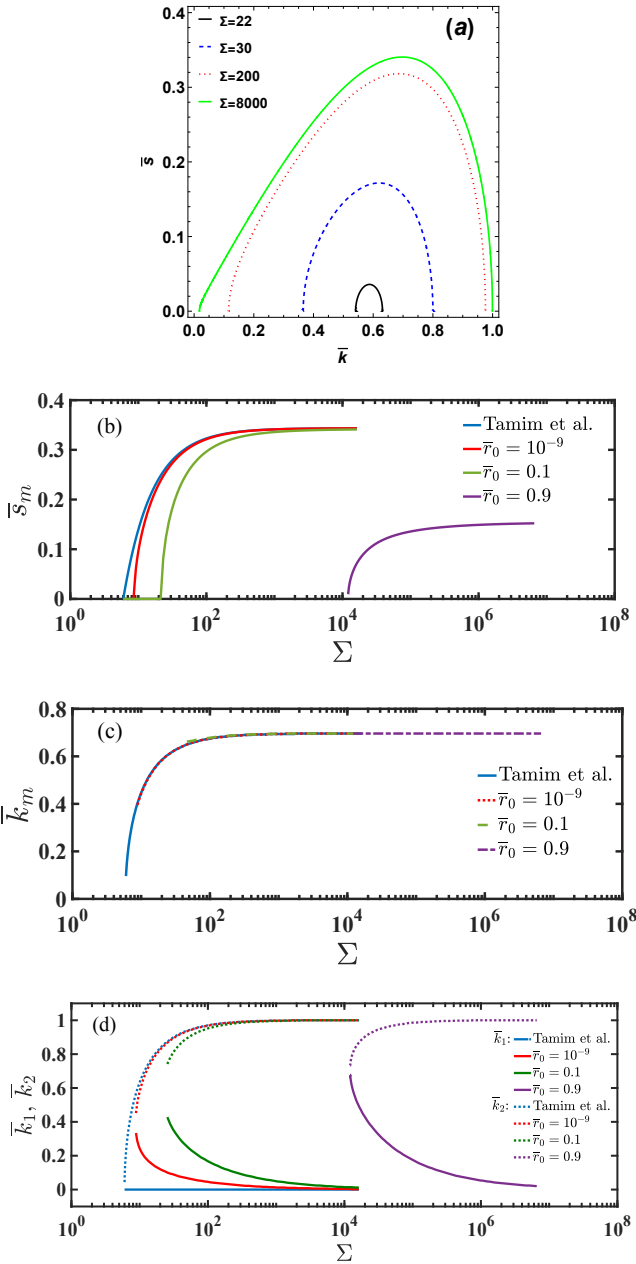


Fig. 2 (a) The dimensionless growth rate \bar{s} as a function of the dimensionless wavenumber \bar{k} for different values of Σ and a fixed $\bar{r}_0 = 0.1$ and $\bar{\tau} = 0$ (purely elastic). (b), (c) and (d): The characteristic quantities \bar{s}_m in (b), \bar{k}_m in (c), and \bar{k}_1 , \bar{k}_2 in (d) as a function of Σ for four different dimensionless rigid core radius, i.e. $\bar{r}_0 = 0$ (from Tamim et al.¹⁵), $\bar{r}_0 = 10^{-9}$, $\bar{r}_0 = 0.1$ and 0.9 . Other parameters: $\bar{\tau} = 0$.

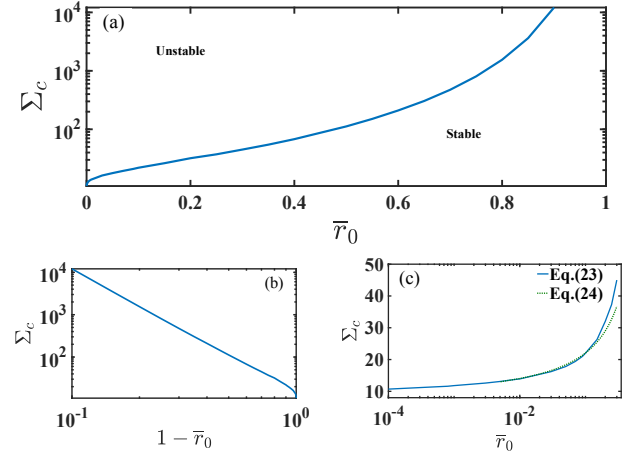


Fig. 3 Stability phase diagram for the purely elastic case, i.e. $\bar{\tau} = 0$. (a) The critical elastocapillary number Σ_c (log scale) as a function of \bar{r}_0 . (b) The critical elastocapillary number Σ_c as a function of $1 - \bar{r}_0$ in log-log scales. (c) A linear-log plot of the critical elastocapillary number Σ_c as a function of \bar{r}_0 .

To show how the onset of instability depends on Σ and \bar{r}_0 , we plot a phase diagram of Σ_c (in log scales) as a function of \bar{r}_0 in Fig. 3 (a). We see that increasing the radius of the rigid cylindrical core or decreasing the elastocapillary number can make the coated film more stable. Hence both the stiffness and the rigid core perform a stabilizing effect. In Fig. 3(b), we plot Σ_c as a function of the thickness of the coated layer, i.e. $\bar{H} = 1 - \bar{r}_0$, in log-log scales. We find that when $\bar{r}_0 \gtrsim 0.2$, the curve follows a power law $\Sigma_c \sim \bar{H}^\lambda$ where $\lambda \approx -2.75$. Hence the critical value Σ_c for a thin coated elastic film is orders of magnitudes larger than a thick film. In the opposite limit of $\bar{r}_0 \rightarrow 0$, we find that our results can be described by a logarithmic relation given as

$$\Sigma_c = \Sigma_{co} - \frac{a}{\log(\bar{r}_0)} \quad (24)$$

where $\Sigma_{co} = 6$ is the critical value for a soft elastic fibre without a rigid cylindrical core obtained by Mora et al.¹² or Tamim et al.¹⁵, and $a = 37$ is a fitting parameter. The comparison is shown in Fig. 3 (c) for small \bar{r}_0 .

4.2 Viscoelastic effects

The dimensionless growth rate \bar{s} as a function of the dimensionless wavenumber \bar{k} for different values of Σ and a fixed $\bar{r}_0 = 0.1$ and $\bar{\tau} = 0$ (purely elastic). (b), (c) and (d):

We study the instability when $\bar{\tau} \neq 0$. We show results for two different rigid cylindrical core radius, namely $\bar{r}_0 = 0.1$ (a thick coated layer) and $\bar{r}_0 = 0.9$ (a thin coated layer). Since the critical elastocapillary numbers for $\bar{r}_0 = 0.1$ and $\bar{r}_0 = 0.9$ are different by orders of magnitude, we take a fixed value of $\Sigma = 50$ for the case

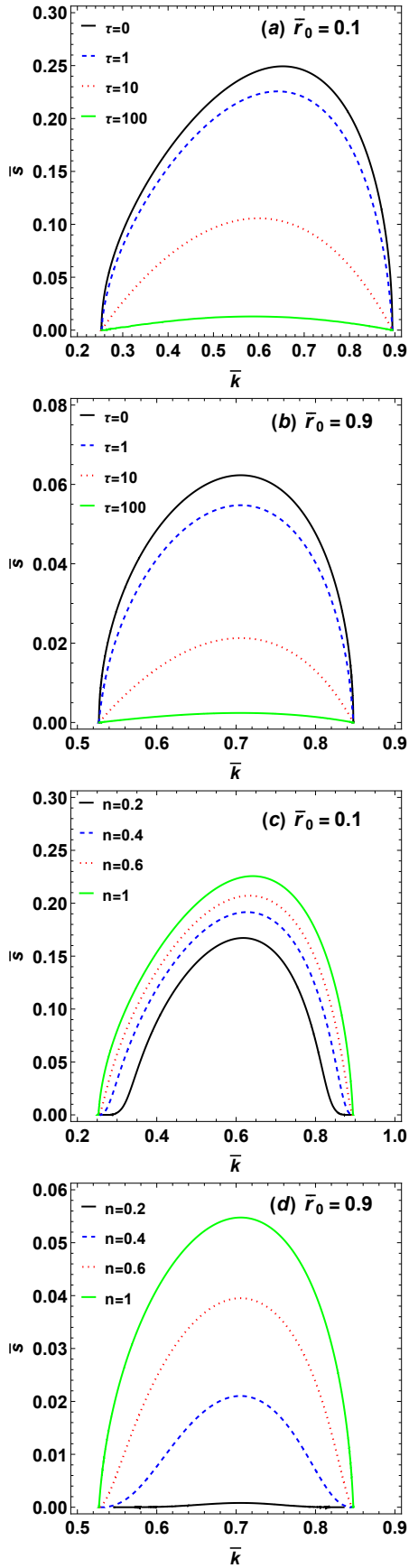


Fig. 4 The dimensionless growth rate \bar{s} as a function of the dimensionless wavenumber \bar{k} for different values of $\bar{\tau}$ and a fixed value of exponent $n = 1$ with $\bar{r}_0 = 0.1$ and $\Sigma = 50$ in (a), and $\bar{r}_0 = 0.9$ and $\Sigma = 15000$ in (b). The dimensionless growth rate \bar{s} vs the dimensionless wavenumber \bar{k} for different values of exponent n and a fixed value of $\bar{\tau} = 1$ with $\bar{r}_0 = 0.1$ and $\Sigma = 50$ in (c), and $\bar{r}_0 = 0.9$ and $\Sigma = 15000$ in (d).

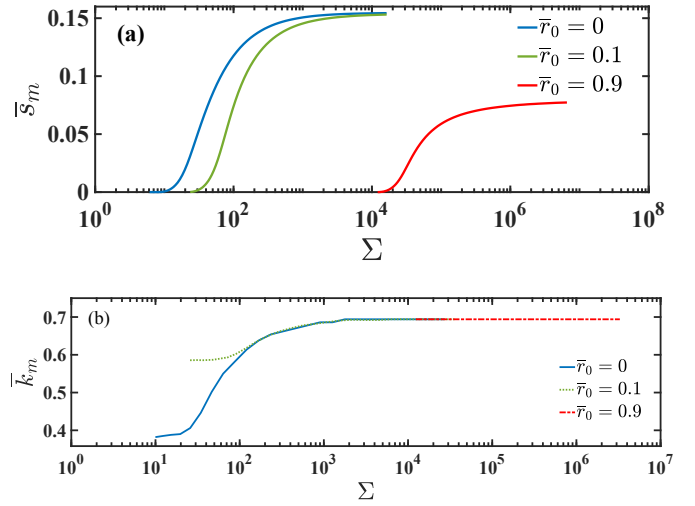


Fig. 5 The characteristic quantities \bar{s}_m in (a) and \bar{k}_m in (b) as a function of Σ for three different dimensionless rigid core radius, i.e. $\bar{r}_0 = 0$ (from Tamim *et al.*¹⁵), $\bar{r}_0 = 0.1$ and 0.9 . Other parameters: $\bar{\tau} = 100$ and $n = 0.5$.

of $\bar{r}_0 = 0.1$ and a fixed value of $\Sigma = 15000$ for the case of $\bar{r}_0 = 0.9$. In Fig.4 (a) and (b), we present the dispersion relation from eqn. (23) for different $\bar{\tau}$ and in Fig.4 (c) and (d) for different n . We see that both \bar{k}_1 and \bar{k}_2 are independent of $\bar{\tau}$ and n . The dimensionless growth rate of the fastest growing mode \bar{s}_m decreases when $\bar{\tau}$ is enhanced. It means that the viscoelastic relaxation of the material slows down the growth of disturbance. We also see that when $\bar{\tau}$ is increased, the dimensionless wavenumber of the fastest growing mode becomes smaller for $\bar{r}_0 = 0.1$ but remains constant for $\bar{r}_0 = 0.9$. When varying the other viscoelastic parameter n , the dimensionless growth rate of the fastest growing mode \bar{s}_m decreases with decreasing \bar{n} . The change of \bar{s}_m with varying \bar{n} is more sensitive for $\bar{r}_0 = 0.9$ than for $\bar{r}_0 = 0.1$ as we can see in Fig.4 (c) and (d). The dimensionless wavenumber of the fastest growing mode \bar{k}_m decreases slightly when n is increased from $n = 0.2$ to $n = 1$ for $\bar{r}_0 = 0.1$ but remains constant for $\bar{r}_0 = 0.9$. Lastly, we take $\bar{\tau} = 100$ and $n = 0.5$, and show the results for \bar{s}_m and \bar{k}_m as a function of Σ for three different $\bar{r}_0 = 0, 0.1$ and 0.9 in Fig.5. We see the behaviors of \bar{s}_m and \bar{k}_m for $\bar{\tau} = 100$ are similar to those shown in Fig.2 (b) and (c) for the purely elastic cases, i.e. $\bar{\tau} = 0$, except when Σ is close to the critical value Σ_c . For $\bar{\tau} = 100$, the critical values Σ_c are the same as for $\bar{\tau} = 0$. However, when Σ is approaching Σ_c , the curves for both \bar{s}_m and \bar{k}_m bend concavely. Moreover, the value of \bar{k}_m becomes dependent on \bar{r}_0 when Σ is around Σ_c .

5 Conclusion

We investigate the onset of the PRI of a soft layer coated on a rigid cylinder by analytically deriving the dispersion relation using the linear stability analysis. We implement the Chasset-Thirion model for the viscoelastic response of the soft layer. We find that the stiffness (characterized by $1/\Sigma$) and the rigid cylindrical core (characterized by \bar{r}_0) perform a stabilizing effect. The dimensionless growth rate of the fastest growing mode \bar{s}_m decreases with decreasing Σ or increasing \bar{r}_0 . Importantly, there exists a critical

elastocapillary number Σ_c for each \bar{r}_0 such that the coated layer is stable for any $\Sigma < \Sigma_c$. The critical value depends strongly on \bar{r}_0 . For example, for $\bar{r}_0 = 0.9$, the soft layer becomes unstable only when the fibre is very soft, namely when $\Sigma \geq 12100$. While for a soft fibre without a rigid core ($\bar{r}_0 = 0$), the onset of instability occurs at $\Sigma \approx 6$, which is three to four orders of magnitudes smaller. This remarkable result would be interesting to be verified by performing experiments for different soft coatings on a fibre. Regarding the dimensionless wavenumber of the fastest growing mode \bar{k}_m , we find that \bar{k}_m decreases with decreasing Σ . Interestingly, \bar{k}_m is independent of \bar{r}_0 for the purely elastic case.

Regarding the roles of the viscoelastic parameters $\bar{\tau}$ and n , we find that increasing the relaxation timescale of viscoelastic material $\bar{\tau}$ or reducing the power n can slow down the growth of disturbance. Changing either $\bar{\tau}$ or n have no effect on the critical elastocapillary number. However, for $\bar{\tau} \neq 0$, the curves for both \bar{s}_m and \bar{k}_m bend concavely when Σ is approaching Σ_c . The value of \bar{k}_m becomes dependent on \bar{r}_0 when Σ is around Σ_c .

6 Appendix: validation of our model

6.1 The Newtonian fluid limit

Our viscoelastic model reduces to the Newtonian fluid when $n = 1$ and in the limits of $\mu_o \rightarrow 0$ and $\mu_o \tau \rightarrow \eta$, where η is the dynamic viscosity of the fluid. In terms of the dimensionless parameters, it means $\Sigma \rightarrow \infty$ and $\Sigma/\bar{\tau} \rightarrow \text{Oh} \equiv \eta/\sqrt{\rho\gamma R}$, where Oh is called the Ohnesorge number. In this limiting situation, the dimensionless governing equation (11) is reduced to

$$\hat{s} \frac{\partial^2 \bar{u}_i}{\partial x_j \partial x_j} - \frac{\partial \bar{p}}{\partial x_i} = \frac{\hat{s}^2 \bar{u}_i}{\text{Oh}^2}, \quad (25)$$

where $\hat{p} \equiv \bar{p}/\Sigma = R\bar{p}/\gamma$ and we have introduced a new rescaled growth rate $\hat{s} \equiv \eta R s/\gamma = \text{Oh} \bar{s}$. The dispersion relation is obtained by substituting $\alpha = \sqrt{\hat{s}/\text{Oh}^2 + \bar{k}^2}$ and $\beta = 1/\hat{s}$ in eq.(23). The dimensionless control parameters are Oh and \bar{r}_0 .

6.1.1 Stokes flow case

Taking further the limit that $\text{Oh} \rightarrow \infty$, eq. (25) reduces to the Stokes equation in Laplace space. The remaining dimensionless control parameters is only \bar{r}_0 . We validate the expression of our dispersion relation (eq. 23) in this limiting case by comparing our results with that from Zhao et al.³⁰ in which the dispersion relation is obtained using the normal mode method to solve the Stokes equations. Fig. 6 shows the comparison for the cases of very small fibre radius ($\bar{r}_0 = 10^{-9}$), thick coated liquid film ($\bar{r}_0 = 0.1$) and thin coated liquid film ($\bar{r}_0 = 0.9$).

Conflicts of interest

“There are no conflicts to declare”.

Acknowledgements

The authors gratefully acknowledges financial support from the Research Council of Norway (Project No. 315110).

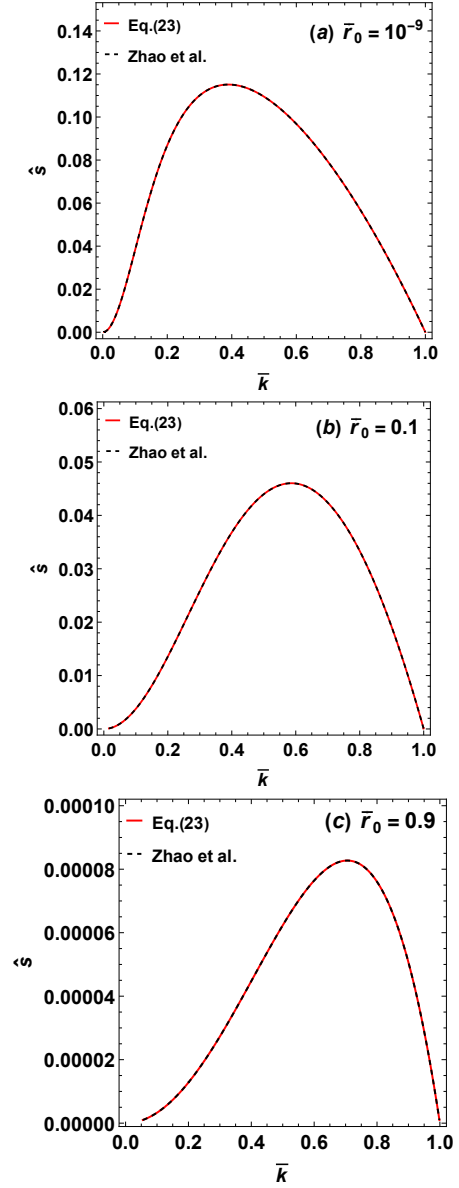


Fig. 6 The dispersion relation between the growth rate \hat{s} and the wavenumber \bar{k} in the Stokes flow limit for $\bar{r}_0 = 10^{-9}$ in (a), $\bar{r}_0 = 0.1$ in (b) and $\bar{r}_0 = 0.9$ in (c). Solid lines: our results when substituting $\alpha = \bar{k}$ and $\beta = 1/\hat{s}$ for eq. (23). Dashed lines: results from Zhao et al.³⁰.

Notes and references

- 1 Y. Guo, J. Bae, Z. Fang, P. Li, F. Zhao and G. Yu, *Chemical Reviews*, 2020, **120**, 7642–7707.
- 2 B. Roman and J. Bico, *Journal of Physics Condensed Matter*, 2010, **22**, year.
- 3 A. Jagota, D. Paretkar and A. Ghatak, *Physical Review E*, 2012, **85**, 051602.
- 4 M. L. Wei, Z., *Europhysics Letters (EPL)*, 2014, **106**, 14002.
- 5 R. W. Style, A. Jagota, C. Y. Hui and E. R. Dufresne, *Annual Review of Condensed Matter Physics*, 2017, **8**, 99–118.
- 6 J. Bico, É. Reyssat and B. Roman, *Annual Review of Fluid Mechanics*, 2018, **50**, 629–659.
- 7 J. A. F. Plateau, *Acad. Sci. Bruxelles Mem.*, 1843, **16**, 3.
- 8 L. Rayleigh, *Proc. Roy. Soc. London*, 1879, **10**, 4.
- 9 J. Eggers and E. Villermaux, *Rep. Progr. Phys.*, 2008, **71**, 036601.
- 10 M. Taffetani and P. Ciarletta, *Physical Review E*, 2015, **E91**, 032413.
- 11 C. Xuan and J. Biggins, *Physical Review E*, 2017, **95**, 1–8.
- 12 S. Mora, T. Phou, J. M. Fromental, L. M. Pismen and Y. Pomeau, *Physical Review Letters*, 2010, **105**, 1–4.
- 13 C. Lestringant and B. Audoly, *Proceedings of the Royal Society A: Mathematical, Physical and Engineering Sciences*, 2020, **476**, 20200337.
- 14 Y. Fu, L. Jin and A. Goriely, *Journal of the Mechanics and Physics of Solids*, 2021, **147**, 104250.
- 15 S. I. Tamim and J. B. Bostwick, *Soft Matter*, 2021, **17**, 4170–4179.
- 16 A. Pandey, M. Kansal, M. A. Herrada, J. Eggers and J. H. Snoeijer, *Soft Matter*, 2021, **17**, 5148–5161.
- 17 B. Dortdivanlioglu and A. Javili, *Extreme Mechanics Letters*, 2022, **55**, 101797.
- 18 G. Yang, C. F. Gao and C. Q. Ru, *International Journal of Solids and Structures*, 2022, **241**, year.
- 19 C. Q. Ru, *Mechanics Research Communications*, 2022, **124**, 103959.
- 20 P. P. Bhat, S. Appathurai, M. T. Harris, M. Pasquali, G. H. McKinley and O. A. Basaran, *Nature Physics*, 2010, **6**, 625–631.
- 21 D. Quéré, *Annual Review of Fluid Mechanics*, 1999, **31**, 347–384.
- 22 H.-C. CHANG and E. A. DEMEKHIN, *Journal of Fluid Mechanics*, 1999, **380**, 233–255.
- 23 I. L. KLIAKHANDLER, S. H. DAVIS and S. G. BANKOFF, *Journal of Fluid Mechanics*, 2001, **429**, 381–390.
- 24 C. RUYER-QUIL, P. TREVELEYAN, F. GIORGIUTTI-DAUPHINÉ, C. DUPRAT and S. KALLIADASIS, *Journal of Fluid Mechanics*, 2008, **603**, 431–462.
- 25 Y. Zheng, H. Bai, Z. Huang, X. Tian, F.-Q. Nie, Y. Zhao, J. Zhai and L. Jiang, *Nature*, 2010, **463**, 640–643.
- 26 S. Haefner, M. Benzaquen, O. Bäümchen, T. Salez, R. Peters, J. D. McGraw, K. Jacobs, E. Raphaël and K. Dalnoki-Veress, *Nature Communications*, 2015, **6**, 7409.
- 27 A. Sadeghpour, Z. Zeng and Y. S. Ju, *Langmuir*, 2017, **33**, 6292–6299.
- 28 H. Chen, T. Ran, Y. Gan, J. Zhou, Y. Zhang, L. Zhang, D. Zhang and L. Jiang, *Nat. Mater.*, 2018, **17**, 935–942.
- 29 H. Ji, C. Falcon, A. Sadeghpour, Z. Zeng, Y. S. Ju and A. L. Bertozzi, *Journal of Fluid Mechanics*, 2019, **865**, 303–327.
- 30 C. Zhao, Y. Zhang and T. Si, *Journal of Fluid Mechanics*, 2023, **954**, 1–22.
- 31 S. L. Goren, *Journal of Fluid Mechanics*, 1962, **12**, 309–319.
- 32 S. L. Goren, *Journal of Colloid Science*, 1964, **19**, 81–86.
- 33 Y. Zhang, S. T. Ellison, S. Duraivel, C. D. Morley, C. R. Taylor and T. E. Angelini, *Bioprinting*, 2021, **21**, e00121.
- 34 M. M. Fitzgerald, K. Bootsma, J. A. Berberich and J. L. Sparks, *Biomacromolecules*, 2015, **16**, 1497–1505.
- 35 D. K. Nandakumar, Y. Zhang, S. K. Ravi, N. Guo, C. Zhang and S. C. Tan, *Advanced Materials*, 2019, **31**, 1806730.
- 36 R. Bar-Ziv and E. Moses, *Phys. Rev. Lett.*, 1994, **73**, 1392–1395.
- 37 E. Hannezo, J. Prost and J.-F. m. c. Joanny, *Phys. Rev. Lett.*, 2012, **109**, 018101.
- 38 D. Gonzalez-Rodriguez, S. Sart, A. Babataheri, D. Tareste, A. I. Barakat, C. Clanet and J. Husson, *Physical Review Letters*, 2015, **115**, 088102.
- 39 M. R. King and S. Petry, *Nature Communications*, 2020, **11**, 270.
- 40 S. U. Setru, B. Gouveia, R. Alfaro-Aco, J. W. Shaevitz, H. A. Stone and S. Petry, *Nature Physics*, 2021, **17**, 493–498.